Deconvolution and measurement of bulk and surface optical absorptions in Ti:Al_2O_3 crystals using photopyroelectric interferometry

Chinhua Wang and Andreas Mandelis[a)]
Photothermal and Optoelectronic Diagnostics Laboratories, Department of Mechanical and Industrial Engineering, University of Toronto, Toronto M5S 3G8, Canada

(Received 19 January 1999; accepted for publication 25 March 1999)

The extension of our earlier single-layer (monolithic) photopyroelectric (PPE) interferometric theory to include surface and bulk optical absorptions has allowed the measurement of both bulk absorption coefficient and surface absorptance in one single experiment. Based on purely thermal-wave interferometry, the thermal-wave cavity lengths of a PPE interferometer were scanned using pairs of Ti: sapphire crystals with appropriate combinations of figure of merit, surface polish, and thickness. In the conventional single-ended (noninterferometric) PPE technique, the surface reflectivity, surface absorptance, and bulk absorption coefficient are always coupled together. However, PPE destructive interferometry provides a method for extracting highly precise values of one of these optical parameters, without the requirement of equally precise knowledge of the values of the others. © *1999 American Institute of Physics.* [S0034-6748(99)02007-9]

I. INTRODUCTION

Photothermal (PT) and photoacoustic (PA) spectroscopic techniques have been used successfully in measurements of optical absorption coefficients and nonradiative quantum efficiencies for a variety of optical materials, including laser crystals.[1–13] Among the various embodiments of PA and PT techniques, photopyroelectric detection (PPE), as pointed out elsewhere,[1–4,10–12,14] has a certain number of advantages. A major advantage of PPE detection over other conventional PT techniques is the fact that one can measure *directly* and *self-consistently* both the optical absorption coefficient, $\beta(\lambda)$, and the nonradiative quantum efficiency, $\eta(\lambda)$.[2,3,12,15,16] Lock-in quadrature photopyroelectric spectroscopy (Q-PPES) was used in a novel noncontact experimental scheme to obtain high-resolution spectra of the nonradiative quantum efficiency of Ti:sapphire laser crystals with widely different figures of merit (FOM).[2] Using the same setup, optical-absorption-coefficient spectra were obtained from the lock-in in-phase (IP) channel in a separate measurement, in the so-called ''purely optical transmission (OT) mode.'' The single-layer (monolithic), single-ended theoretical model,[2] however, allowed only the determination of total absorptance (bulk and surface) values. Subsequently, Vanniasinkam *et al.*[3] separated the surface absorptance from the bulk absorption coefficient in a modified PPE theory. Those authors employed two samples of identical bulk quality and surface treatment, but different thicknesses and performed two independent PPE experimental measurements in the conventional single-ended configuration. The contributions from the surface and the bulk were thus separated from each other. It was shown,[3,11,12] however, that the sensitivity of conventional single-ended PPE measurements suffers from a large baseline signal, generated by the direct transmission to the detector surface of the incident radiation through the transparent sample under investigation. With regard to transparent materials, this large baseline signal, which appears in the lock-in IP channel, is much larger than that of the *Q* channel, by more than two orders of magnitude.[3] As a result, one must choose a very low instrumental sensitivity to prevent the lock-in amplifier from overloading due to this large baseline signal. Usually, this operation limits the dynamic range of the PPE measurement, which is far too low to detect small changes in both IP and *Q* channels where high quality laser crystals are concerned, with minute differences in optical properties. Moreover, in comparing different crystals, it is difficult to ensure identical alignment procedures for the two individual measurements. Regarding accuracy, the PPE measurement of $\beta(\lambda)$ in the single-ended purely optical transmission mode is actually a single-point measurement at a specific wavelength. The one-point measurement thus lacks the accuracy afforded by linear correlation and averaging process, and the measurement depends directly on other optical parameters, such as surface reflectivity of the sample. Very recently, a PPE interferometric technique was introduced and applied to the coherent suppression of the large baseline signal for the characterization of transparent samples, as well as for the study of the thermophysical properties of intracavity gases.[17–19] The figure of merit for the large baseline suppression, defined as the single-ended-to-interferometric signal amplitude ratio, was found to be over 3×10^3 in practice, with a 5 mW laser source.[18] The measurement precision, signal dynamic range and signal-to-noise ratio (SNR) were also much improved over the single-ended configuration with the thermal-wave interferometric technique. One of the earlier experimental results shows the difference in total (bulk and surface) optical absorption coefficients between a pair of nominally identical BK7 window glasses using our monolithic PPE interferometric theory.[18] It is believed, however, that this difference in the total absorption coefficient is mainly due to the difference between the surface absorptan-

a)Electronic mail: mandelis@mie.utoronto.ca

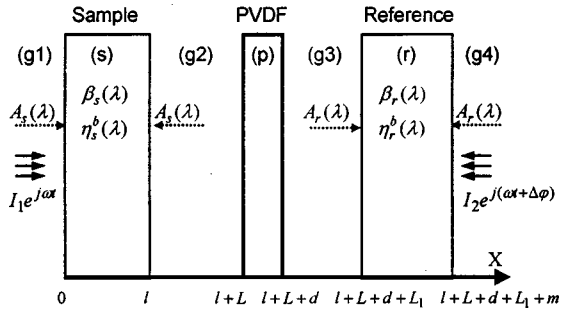

FIG. 1. Schematic of the photopyroelectric interferometric setup for the theoretical analysis. Bulk optical absorption coefficients of sample and reference, respectively: $\beta_s(\lambda),\beta_r(\lambda)$; nonradiative energy conversion efficiency of sample and reference, respectively: $\eta_s^b(\lambda),\eta_r^b(\lambda)$; surface absorptance of sample and reference, respectively: A_s,A_r; thickness of sample and reference, respectively: l,m; thickness of PVDF detector: d; sample-PVDF and PVDF-reference cavity lengths, respectively: L,L_1.

ces of the two samples as a result of the antireflection coating optical properties rather than due to the difference in bulk optical properties. In addition, investigations which have studied the impact of the quality of laser crystal rods on output efficiency[10,20,21] have demonstrated an intimate correlation between the slope efficiency and lasing threshold and the quality of the laser crystal, including bulk crystal preparation and surface polish. Therefore, the requirement for improved control and evaluation of bulk optical properties of laser crystals as a function of preparation, as well as the effects of surface polish, motivates the deconvolution of surface absorptance from that of the bulk using our novel PPE interferometric technique. In this article, the PPE interferometric theory[18] is extended to separately include the surface and bulk absorption in an optical material. The extended theory is then applied to high-precision measurements performed with various combinations of Ti sapphire laser crystals with different figures of merit, polishes, and thicknesses.

II. THEORY

In the interferometric configuration of Fig. 1, two laser beams of intensities I_1 and I_2, respectively, are split off from a laser source and are modulated at the same angular frequency (ω). They have a fixed, adjustable phase shift ($\Delta\varphi$), and are incident onto the front and rear surfaces of a polyvinylidene fluoride (PVDF) thin film detector, passing through optically transparent sample and reference media, which, along with the PVDF sensor in the middle form the thermal-wave cavities $g2$ and $g3$ as shown in Fig. 1. The PVDF detector used in this work has a thickness of 52 μm and is coated with Ni–Al alloy on both sides acting as electrodes. The thickness of each electrode is about 80 nm, thus, it is nearly opaque at 632.8 nm of incident laser light. In our calculations, the optical absorption coefficient of the electrodes was considered infinite. The incident beams are assumed to illuminate the PVDF sensor uniformly with spot-sizes much larger than the thermal diffusion length in PVDF, so that the one dimensionality of the heat transfer model is assured. The photopyroelectric signal from the PVDF detector is proportional to the average ac temperature of the PVDF film detector.[1] It is governed by coupled one-dimensional heat diffusion equations subject to appropriate boundary conditions of thermal-wave field continuity and flux conservation across each interface ($g1$-s, s-$g2$, $g2$-p, p-$g3$, $g3$-r, and r-$g4$) of Fig. 1. Assuming the whole system is exposed to the same gaseous atmosphere (usually, air), the appropriate thermal-wave equations have the form:

$$\frac{d^2T_i(x)}{dx^2}-\sigma_i^2T_i(x)=0,$$

$$i=1,2,3,4,p \quad \text{for regions } g1,\ g2,\ g3,\ g4, \text{ and } p, \tag{1a}$$

$$\frac{d^2T_s(x)}{dx^2}-\sigma_s^2T_s(x)=-\eta_s^b\beta_s\frac{I_{ts}(x)}{2k_s}, \quad 0\leqslant x\leqslant l, \tag{1b}$$

$$\frac{d^2T_r(x)}{dx^2}-\sigma_r^2T_r(x)=-\eta_r^b\beta_r\frac{I_{tr}(x)}{2k_r},$$

$$l+L+d+L_1\leqslant x\leqslant l+L+d+L_1+m. \tag{1c}$$

In Eqs. (1), $\sigma_i=(1+j)\sqrt{\omega/2\alpha_i}$ is the complex thermal diffusion coefficient in spatial region i ($i=g1,g2,g3,g4,s,p,r$) with thermal diffusivity α_i; k_s,k_r is the thermal conductivity of the sample and the reference, respectively; $I_{ts}(x),I_{tr}(x)$ are the total optical fluence contributions to depth x in the sample and in the reference, respectively.[2] They have been derived upon considering the multiple reflections of the incident and the reflected light by the metal electrode(coating) of the detector back into the sample and the reference, and are given as follows:

$$I_{ts}(x)=I_1\frac{(1-R_s)e^{-A_s}}{1-R_s^2e^{-2(\beta_sl+A_s)}}(N_1e^{-\beta_sx}+N_2e^{-\beta_s(2l-x)}), \tag{2a}$$

$$I_{tr}(x)=I_2e^{j\varphi}\frac{(1-R_r)e^{-A_r}}{1-R_r^2e^{-2(\beta_rm+A_r)}}\times(N_{1r}e^{-\beta_r(l+L+d+L_1+m-x)}+N_{2r}e^{-\beta_r[2m-(l+L+d+L_1+m-x)]}). \tag{2b}$$

Here, R_s,R_r,R_p are the surface reflectances of the sample, of the reference, and of the PVDF detector, respectively. N_1,N_2 and N_{1r},N_{2r} are combinations of constants including surface absorptance, bulk absorption coefficient, sample and reference thickness. The detailed expressions are given in the Appendix. The solutions of the foregoing thermal-wave equations contain coupled constants via the boundary conditions of temperature continuity (absence of interfacial thermal resistance) and heat flux discontinuities at four surfaces of the sample and the reference (presence of infinitesimal thin absorbing layers acting like interfacial sources). To formulate the heat flux conservation relations, the thermal-wave Eqs. (1b) and (1c) are integrated over a surface layer of thickness $\epsilon\to 0$ at each of four surfaces of the sample and the reference,[3] respectively:

$$k_g\frac{dT_1(x)}{dx}-k_s\frac{dT_s(x)}{dx}=\eta_s^{(0)}A_sI_t(0), \quad x=0, \tag{3a}$$

$$k_s\frac{dT_s(x)}{dx}-k_g\frac{dT_g(x)}{dx}=\eta_s^{(0)}A_sI_t(l),\quad x=l, \tag{3b}$$

$$k_g\frac{dT_3(x)}{dx}-k_r\frac{dT_r(x)}{dx}=\eta_r^{(0)}A_rI_{tr}(m),\quad x=l+L+d+L_1, \tag{3c}$$

$$k_r\frac{dT_3(x)}{dx}-k_g\frac{dT_g(x)}{dt}=\eta_r^{(0)}A_rI_{tr}(0),\quad x=l+L+d+L_1+m, \tag{3d}$$

where $I_t(0)$, $I_t(l)$, $I_{tr}(0)$, and $I_{tr}(m)$ are constants related to β_s,β_r,A_s,A_r. They are given in the Appendix. At each surface of the sample and the reference, the absorptance and the nonradiative energy conversion efficiency is defined as

$$A_i\equiv\lim_{\epsilon\to 0}(\beta_i\epsilon),\quad i=s,r \tag{4}$$

and

$$\eta_i^{(0)}\equiv\lim_{\epsilon\to 0}\eta_i^{(\epsilon)},\quad i=s,r, \tag{5}$$

where ϵ is the effective thickness of the surface layer. Equations (3a)–(3d) replace the thermal flux continuity boundary conditions at material surfaces used in Ref. 18. The thermal flux discontinuities at the surfaces of the pyroelectric detector are

$$k_g\frac{dT_2(x)}{dx}-k_p\frac{dT_p(x)}{dx}=(1-R_p)I_1(l),\quad x=l+L, \tag{6a}$$

$$k_p\frac{dT_p(x)}{dx}-k_g\frac{dT_3(x)}{dx}=(1-R_p)I_2(m),\quad x=l+L+d, \tag{6b}$$

where $I_1(l)$ and $I_2(m)$ represent the incident beam intensities at the front and rear surfaces of the PVDF thin film, respectively. They are given in detail in the Appendix. Following the algebraic procedure of Ref. 18, we finally obtain a modified expression for the photopyroelectric interferometric signal associated with the geometry of Fig. 1:

$$V(\omega)=\frac{S(\omega)}{\sigma_p(1+b_{gp})}\times\frac{H_1G_1(1+W_{21}e^{-2\sigma_gL})+H_2G_2(1+V_{34}e^{-2\sigma_gL_1})+2b_{gp}(H_1G_3e^{-\sigma_gL}+H_2G_4e^{-\sigma_gL_1})}{e^{\sigma_pd}(1+\gamma_{gp}V_{34}e^{-2\sigma_gL_1})(1+\gamma_{gp}W_{21}e^{-2\sigma_gL})-e^{-\sigma_pd}(\gamma_{gp}+W_{21}e^{-2\sigma_gL})(\gamma_{gp}+V_{34}e^{-2\sigma_gL_1})}. \tag{7}$$

$S(\omega)$ is the instrumental transfer function. It can usually be normalized out experimentally. In addition,

$$b_{ij}=k_i\sqrt{\alpha_j}/k_j\sqrt{\alpha_i}, \tag{8a}$$

$$\gamma_{ij}=(1-b_{ij})/(1+b_{ij}), \tag{8b}$$

$$W_{21}=-\gamma_{gs}\frac{e^{\sigma_sl}-e^{-\sigma_sl}}{e^{\sigma_sl}-\gamma_{gs}^2e^{-\sigma_sl}}, \tag{8c}$$

$$V_{34}=-\gamma_{gr}\frac{e^{\sigma_rm}-e^{-\sigma_rm}}{e^{\sigma_rm}-\gamma_{gr}^2e^{-\sigma_rm}}, \tag{8d}$$

$$G_1=\frac{(1-R_p)}{k_p\sigma_p}\times\frac{I_1(1-R_s)^2e^{-(\beta_sl+2A_s)}}{1-R_s^2e^{-2(\beta_sl+A_s)}}, \tag{8e}$$

and

$$G_2=\frac{(1-R_p)}{k_p\sigma_p}\times\frac{I_2e^{j\Delta\varphi}(1-R_r)^2e^{-(\beta_rm+2A_r)}}{1-R_r^2e^{-2(\beta_rm+A_r)}}. \tag{8f}$$

Expressions for H_1,H_2 and G_3,G_4 are given in the Appendix. From the structure of the PPE output voltage of Eq. (7), it is obvious that the overall output signal is the result of the complex (vectorial) superposition of the thermal-wave fields within the PVDF detector generated by three sources: (1) direct transmission of the incident light passing through the sample and the reference [the H_1G_1 and H_2G_2 terms in the numerator of Eq. (7)]; (2) thermal-wave confinement within the cavity formed by the sample and the reference [W_{21} and V_{34} terms in the numerator of Eq. (7)]; and (3) nonradiative (optical-to-thermal) conversion processes of the sample and the reference following optical absorption. These occur in bulk and at the surface [H_1G_3 and H_2G_4 terms in the numerator of Eq. (7)]. Theoretical simulation shows that the contribution from the third source is much smaller (~3–4 orders of magnitude less) than that from the first and the second sources for highly transparent materials.[19] Therefore, the third source has been neglected in the quantitative analyses of our data. If $A_s=0$ and $A_r=0$, the PPE output of Eq. (7) reduces to the monolithic expression, Eq. (5), of Ref. 18, as expected.

It can be seen that the overall output PPE signal of Eq. (7) is affected by the surface absorptances as well as by the bulk absorption coefficients of the sample and the reference. By using appropriate combinations of pairs of samples, in which only one parameter (surface absorptance, bulk absorption or thickness), varies between a sample-reference pair, one may precisely measure the variation of *this parameter* without requiring accurate information about the values of other parameters. This advantage is attributed to the nature of the destructive interferometric measurement, in which contributions from the same optical/thermal property are coherently canceled within the PVDF detector, while only the signal difference due to small variations in one parameter appears. In contrast, the optical parameters of the sample are always inherently coupled together in the single-ended PPE measurements. Therefore, in the single-ended configuration, one must know all other parameters in order to measure one of them, and the measurement precision is limited by the precision associated with this knowledge. Instrumentally, the coherent noise cancellation within the single detector in the interferometric PPE method is superior to conventional differential optical measurements,[22] in which electronic noise components owing to the employment of two photonic de-

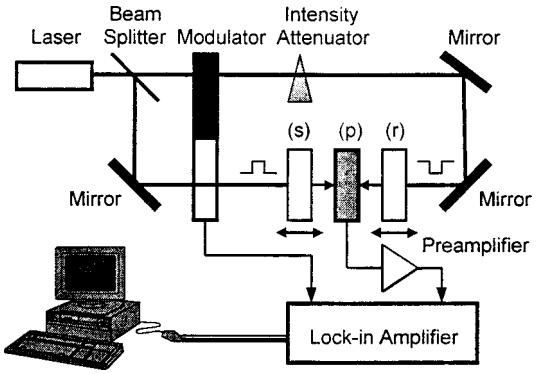

FIG. 2. Experimental setup for PPE thermal-wave interferometry. *s*: sample; *p*: PVDF detector; *r*: reference.

tectors and an electronic signal ratioing amplifier, add, rather than cancel out.

III. EXPERIMENTAL AND RESULTS

A. Experimental setup

The PPE interferometric setup has been described previously.[17–19] A schematic is shown in Fig. 2. At the heart of this interferometer lie two thermal-wave cavities formed by sample-pyroelectric and pyroelectric-reference compartments. The PVDF thin film detector, 52 μm thick and 2 cm in diameter, was installed on an aluminum-base bearing a hole. The PVDF element acts as a thermal-wave signal transducer and as a wall for front and back thermal-wave cavities. Both sample and reference are mounted on a three-dimensional (3D) angularly and linearly adjustable micrometer stage of 10 μm resolution in linear motion and 0.1° in angular rotation. The relative intensities of the front and back incident beams, which are split off of a He–Ne laser ($\lambda = 632.8$ nm, $P \approx 5$ mW), are adjusted by a linear intensity attenuator, and the phase shift between the two beams is precisely controlled by a mechanical chopper (EG&G Model 192), also fixed on a micrometer stage. The experimental data are collected by a PC via a lock-in amplifier (EG&G Model 5210). Several pairs of Ti-sapphire crystals were used in the role of sample and reference in our experiments. For each pair of crystals, only one parameter was different: either the surface absorptance, or the bulk absorption coefficient, or the thickness. The reference was fixed in either the OT (purely optical mode) or the PPE mode,[1] depending on the difference between the sample and the reference. The sample-PVDF cavity length was scanned. By fitting the scanning curves (amplitude and phase) to Eq. (7) for each pair of sample-reference combination, measurements of the desired parameters were obtained.

B. Sample description and preparation

The Ti-sapphire crystals used in this work were grown by the Czochralski pulling technique at Union Carbide, Washougal, WA. Four pairs of crystals with different FOM, different surface polish treatments, and different thicknesses were measured. The FOM in Ti^{3+}:Al_2O_3 is defined as the ratio of the absorption coefficient at the absorption peak (490 nm) to that at the emission peak (820 nm).[3] A high FOM implies a high-quality bulk. Laser-rod grade materials are characterized by FOM ~1000.

1. Samples with identical bulk but different surface quality

Two samples with the same FOM (=800) were measured. One sample did not have optimal (henceforth, ''nonoptimal'') surface polish, and thickness=0.0810 cm; the other sample had laser-rod-grade (''good'') polish and thickness=0.0771 cm. Both samples had been cut from the same Ti sapphire rod and were subjected to the same crystal growth procedure, including post-growth anneal. The nonoptimal crystal was polished with a diamond paste containing 5 μm size particulates. The ''good'' crystal was polished with the best available surface mechanical polish, using a diamond paste with 1 μm size particulates, followed by a further mechanical polish using 0.25 μm size diamond particulates.

2. Samples with different bulk but identical surface quality

Two samples (FOM=40, thickness=2.017 cm; and FOM=800, thickness=2.013 cm) were used. They were subjected to the same nonoptimal surface polishing process as described above. The difference in bulk optical quality was due to difference in growth processes. The two crystals were grown in an identical manner using the Czochralski technique. Then, the FOM=800 sample was subjected to further annealing, thereby removing bulk optical defects present in the unannealed crystal.[2]

3. Samples with identical bulk and surface quality but different thickness

Two pairs of samples were used. The first pair included samples of thicknesses 0.0810 and 0.7929 cm, of the same FOM (=800), and the same nonoptimal surface polish. The second pair consisted of samples of thicknesses 0.0771 and 1.0677 cm, of bulk FOM=800, and the same ''good'' surface polish, as described above.

C. Results

Each pair of the Ti:sapphire samples was measured, with one crystal acting as the sample and the other crystal acting as the reference. The general experimental procedure for all the measurements was as follows: The relative intensities and the phase shift between the two incident beams were adjusted, such that the demodulated lock-in output equaled zero before the sample and the reference were put into place. This procedure makes the PPE system operate in the fully destructive interferometric mode when both the sample and the reference are absent, i.e., $I_1 = I_2$, and $\Delta\varphi = 180$. The sample and the reference were then inserted into the optical path. For each measurement, the cavity length between the sample and the PVDF detector was scanned between the thermally uncoupled and strongly coupled limits.

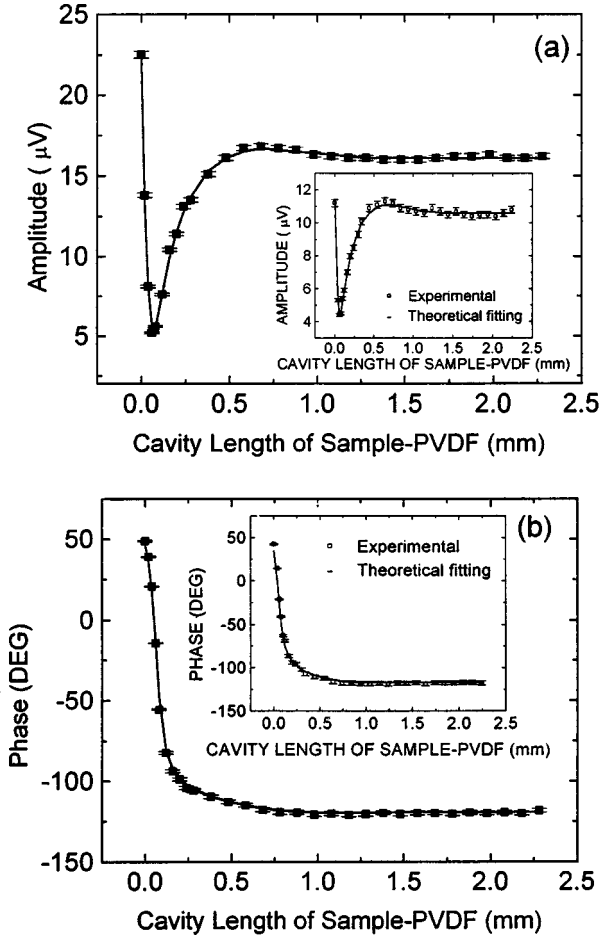

FIG. 3. Experimental and theoretical (fitted) results of (a) the amplitude and (b) phase for a pair of Ti:sapphire crystals with identical bulk optical properties (FOM), but different surface polish. Solid squares: experimental; solid lines: theoretical fits. Insets: experimental and theoretical fit results for the same pair of samples, when the reference was placed farther away from the PVDF sensor (relatively shallow PPE mode).

The reference was fixed in either the thermally uncoupled or fully coupled mode, depending on the particular sample pair combination.

To study samples with identical bulk quality but different surface preparation, the crystal with good surface polish (thickness $l=0.0771\,\mathrm{cm}$) was used as the sample, and the crystal with nonoptimal polish (thickness $m=0.0810\,\mathrm{cm}$) was used as the reference. Known parameters of the sample and the reference are:[2] $\alpha_s=\alpha_r=0.106\,\mathrm{cm^2/s}$, $k_s=k_r=0.33\,\mathrm{W/cm\,K}$, $R_s=R_r=0.07$, and $\beta_s=\beta_r=0.04\,\mathrm{cm^{-1}}$. The modulation frequency was $f=26.5\,\mathrm{Hz}$. Figure 3 shows the scanning curves of the PPE (a) amplitude and (b) the phase when the reference was placed in the deep PPE mode (very close to the PVDF detector). By fitting the experimental data of the amplitude channel to the theoretical formula Eq. (7), the difference in surface absorptance between the sample and the reference ($\Delta A=A_r-A_s$) was found to be 0.0113 ± 0.0002. The cavity length, L_1, between the PVDF film and the reference was $0.213\pm0.002\,\mathrm{mm}$, the average of three measurements. The PPE phase was then calculated using ΔA and L_1 obtained from the amplitude fit to ascertain consistency and validity. The multiparameter fit allows for four parameters to be calculated *uniquely* from Eq. (7): $S(\omega)$; ΔA; absolute value of L_1; and ΔL, a correction for zero separation between the sample and the surface of the detector, which was used to yield absolute value of L, i.e., L is equal to the experimental position plus the offset value ΔL.

To check the sensitivity and to validate the measurement, the reference was subsequently moved farther away from the detector by 0.05 mm, i.e., it was set in a relatively shallow PPE mode. The measurement curves are shown in the insets of Figs. 3(a) and 3(b) for the amplitude and the phase, respectively. The fitted values for ΔA and L_1 at this position were 0.0116 ± 0.0005 and $0.267\pm0.003\,\mathrm{mm}$, respectively. It was therefore concluded that both measurements gave very consistent values, the relative error between the two measurements being only 2.7% for ΔA. The fitted value *difference* for the cavity length L_1 between the two measurements is 0.054 mm, in excellent agreement with the actual scanned distance of 0.05 mm. In view of the experimental readout error from the 10 μm resolution micrometer stage, the reliability of the theoretical fits was judged to be excellent. As regards the SNR and reproducibility, it is noted that the deep PPE mode (short L_1) is better than the shallow PPE mode (longer L_1), due to the higher signal levels resulting from better thermal-wave confinement (higher thermal-power density) inside the cavity in the former configuration.

In the foregoing fitting process, the bulk absorption coefficient and the surface reflectivity of the sample (which was the same as that of the reference), were set to be 0.04 $\mathrm{cm^{-1}}$ and 0.07, respectively. However, it was found that the fitted ΔA value changes from 0.0113 to 0.0099, only a ~4% variation, when the value of the bulk absorption coefficients $\beta_s(=\beta_r)$ was varied from 10^{-8} to 0.4 $\mathrm{cm^{-1}}$, in the case of the two samples with different thickness ($l=0.0771\,\mathrm{cm}$, $m=0.0810\,\mathrm{cm}$). Further simulations showed that the fitted ΔA value is substantially independent of the value of the bulk absorption coefficient $\beta_s(=\beta_r)$, if the thicknesses of the sample and the reference are identical. This is an important feature of the interferometric PPE technique. It implies that for the purpose of measuring the difference of surface absorptances between two crystals of the same (or nearly equal) thickness and bulk optical quality, it is not necessary to know the exact value of the bulk absorption coefficient. A similar observation was made regarding surface reflectivity ($R_s=R_r$): the fitted value of ΔA changes from 0.0118 to 0.0111 (~5.9%) when the values of $R_s(=R_r)$ are varied between 0.02 and 0.08. This can be attributed to the thermal-wave destructive interferometric effect, due to which equal variations of the same parameter in both materials are cancelled to the large extent. In practice, it would be helpful to choose two thin samples in order to minimize the effect of the bulk absorption coefficient to the overall absorptance and to increase the tolerance of the thickness difference between the sample and the reference. Thus, the dependence of the fitted value ΔA on the initial value of the bulk absorption coefficient ($\beta_s=\beta_r$) becomes trivial.

To study samples with different bulk optical properties, but identical surface preparation, one Ti sapphire crystal (FOM=800) of thickness $l=2.013\,\mathrm{cm}$ was used as the sample. The other crystal (FOM=40) of thickness m

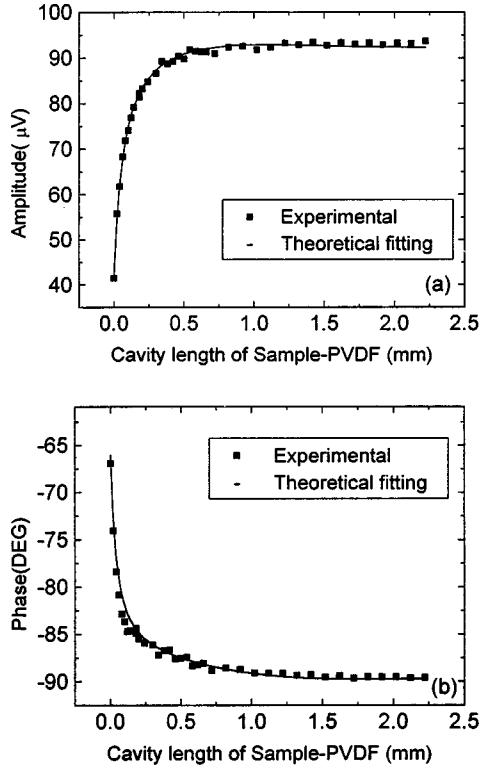

FIG. 4. Experimental and theoretical (fitted) results of (a) the amplitude and (b) phase for a pair of Ti:sapphire crystals with identical surface polishes, but different bulk optical properties (FOM).

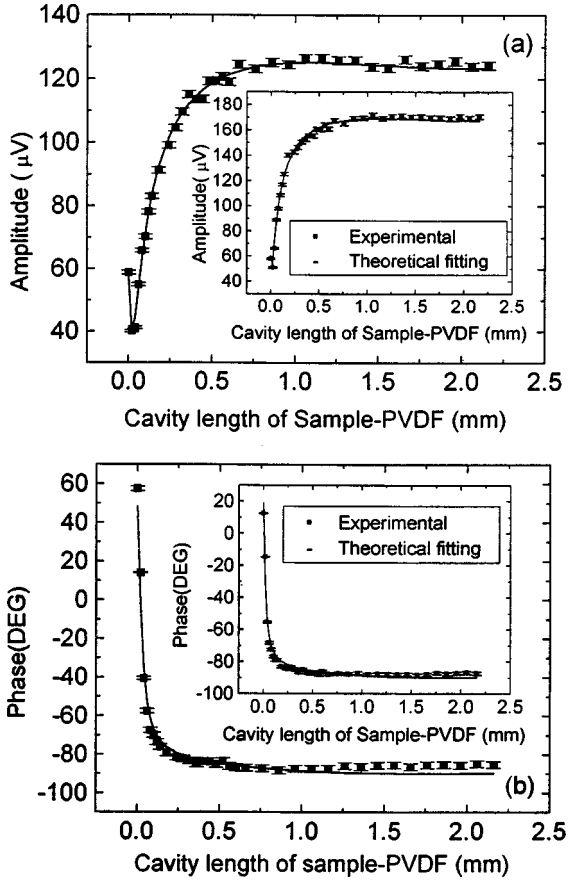

FIG. 5. Experimental and theoretical (fitted) results of (a) the amplitude and (b) phase for a pair of Ti:sapphire crystals of identical bulk optical properties (FOM) and surface (''nonoptimal'') polish, but different thicknesses ($l=0.0810$ cm; $m=0.7929$ cm). Solid squares with error bar: experimental data; solid lines: theoretical fits. Insets: experimental and theoretical (fitted) curves for another pair of crystals with identical bulk optical properties (FOM) and surface (''good'') polish, but different thicknesses ($l=0.0771$ cm, $m=1.0677$ cm).

$=2.017$ cm was used as the reference. The modulation frequency was 10 Hz. Figures 4(a) and 4(b) show the experimental results and the theoretical fits, when the reference was placed in the thermally uncoupled (OT) mode. In practice, this occurs when the reference cavity length L_1, Fig. 1, is greater than 3 mm. The use of the large-cavity-length OT mode for the reference cavity is dictated by the appearance of the sharp minimum in the signal amplitude, when the total absorptances of sample and reference are close to each other, e.g., Fig. 5(a). The line shape and position of the minimum are used as a sensitive measure for material property calculations. This minimum does not appear when the reference cavity length decreases, so that thermal confinement affects the signal (PPE mode).

In Fig. 4, the experimental amplitude data were fitted to the theoretical formula Eq. (7) using the following parameters: $A_s=A_r=0.05$ and $R_s=R_r=0.07$. The other parameters are the same as those used in Fig. 3. The difference of the bulk absorption coefficient between the FOM$=40$ and the FOM$=800$ Ti: sapphire crystals was found to be: $\Delta\beta=\beta_r-\beta_s=0.0545\pm0.0006\,\mathrm{cm}^{-1}$, the average of three measurements. The cavity length L_1 was found to be greater than 8 mm for all three measurements. This best-fit result is consistent with the experimental arrangement, in which the reference was actually placed in OT mode. Both amplitude and phase fits to the data are excellent, as shown in Figs. 4(a) and 4(b). The computational procedure conducted by using different values of surface absorptance $A_s(=A_r)$ and surface reflectivity $R_s(=R_r)$ found that the change in the fitted value of $\Delta\beta$ was only 2.1% (from 0.0552 to 0.0540 cm^{-1}) and 2.2% (from 0.0549 to 0.0537 cm^{-1}), respectively, when A_s was changed from 10^{-5} to 10^{-1} and R_s was changed from 0.02 to 0.13. Once again, it is shown that the measurement of bulk $\Delta\beta$ does not depend strongly on the absolute values of surface absorptance and reflectivity over wide ranges of A_s and R_s. From a different viewpoint, the difference in bulk absorption coefficients between a sample and a reference crystal can be precisely measured without accurate knowledge of the surface absorptance and reflectivity values. It should be noted that the absence of the minimum (''dip'') in Fig. 4(a), unlike Fig. 3(a), is caused by the large difference in transmitted radiation past the sample and the reference crystals, owing to their very different bulk absorption coefficients. Therefore, the interference between the two thermal-wave fields cannot become destructive (or nearly so). Furthermore, the thermal-wave power confinement effect between the sample and the PVDF detector at short cavity lengths is not sufficiently strong to compensate for such a large signal difference caused by the direct optical transmissions on both sides of the detector.

Finally, two pairs of crystals were measured, each pair with identical bulk optical properties (FOM$=800$) and surface preparation (polish), but with different thicknesses. One

pair (thicknesses $l=0.0810$ cm and $m=0.7929$ cm) had the same nonoptimal polish; the other pair (thicknesses $l=0.0771$ cm and $m=1.0677$ cm) had the same good polish. For each pair, the thicker sample was employed as the reference and was placed in the OT mode. The modulation frequency for both cases was $f=10$ Hz. The measurement scans (amplitudes and phases) are shown in Figs. 5(a) and 5(b). By fitting the experimental amplitude of one pair to the Eq. (7), the *absolute* bulk absorption coefficient of the two crystals was found to be: $\beta_s(=\beta_r)=0.0613\pm0.0004\,\mathrm{cm}^{-1}$, the average of three independent measurements. The multiparameter fits yielded the cavity length $L_1>3$ mm for all three measurements. The values of surface absorptance and reflectivity were assumed to be: $A_s=A_r=0.06$, and $R_s=R_r=0.07$, respectively. Similarly, the absolute bulk absorption coefficients for the other pair were found to be: $\beta_s(=\beta_r)=0.0604\pm0.0006\,\mathrm{cm}^{-1}$, and $L_1>8$ mm. The values obtained for the cavity length L_1 are consistent with the experimentally selected OT mode for the reference. It is interesting to note that the calculated absolute bulk absorption coefficients of the two pairs of crystals were in excellent agreement, the relative error between the two measurements being only about 1.5%.

Similar to earlier findings, the fitted results for $\beta_s(=\beta_r)$ do not depend strongly on the values of $A_s(=A_r)$ and $R_s(=R_r)$: the β_s value changed from 0.0619 to 0.0602 cm^{-1} ($\sim$2.7%) with A_s variations between 6×10^{-4} and 10^{-1}; β_s changed from 0.0617 to 0.0603 cm^{-1} ($\sim$2.3%) with R_s variations between 0.01 and 0.12. Therefore, again, it may be concluded that the (common) absolute bulk absorption coefficient of a crystal pair can be obtained precisely by means of PPE destructive interferometry, using two samples with different thicknesses. In the present case, the total thermal-wave fields at both sides of the PVDF detector for both pairs of samples were just close enough to produce a minimum in the amplitude of Fig. 5(a) and its inset when the reference is in the OT mode. This would not be the case when the reference is placed in the PPE mode for these two pairs of samples.

IV. DISCUSSION

A. Effect of PVDF—reference-solid separation (reference cavity length)

The experimental results, shown in Figs. 3, 4, and 5, indicate that the PPE signal can be affected by the operating (OT or PPE) mode of the reference. The selection of the reference-PVDF distance in terms of thermal thickness of the intracavity gas (air) layer,[1] should be guided by the goal to minimize the intensity differences between the thermal-wave fields caused by the directly transmitted light on both sides of the PVDF detector, so as to improve the quality of the measurements. For a pair of samples with relatively large difference in optical absorptances, caused either by surface, bulk, or geometrical parameters, the OT mode for the reference is optimal. This is so, because the thermally thick gas layer in the reference cavity does not introduce a thermal component to the reference signal to offset the thermal confinement in the sample cavity. This allows the latter to exhibit its maximum effect in the form of the observed overall PPE signal minimum. On the other hand, for a pair of samples with relatively small differences in optical absorptance, a thermally thin reference cavity length (the PPE mode) is preferred. Figure 6 shows theoretical curves justifying this statement at $f=26.5$ Hz. The parameters used in that simulation are the same as those in Fig. 3 with $\Delta A=0.0113$. From this simulation it can be seen that the deepest PPE mode (shortest reference cavity length; $L_1=0.1$ mm) gives the sharpest interferometric dip in the amplitude channel and the largest dynamic range in the phase channel. Therefore, higher quality measurements can be expected by using strongly thermally thin reference cavities, from the point of view of the superior signal-to-noise ratio and the resulting precision of the fitting process, as discussed in relation to Fig. 3.

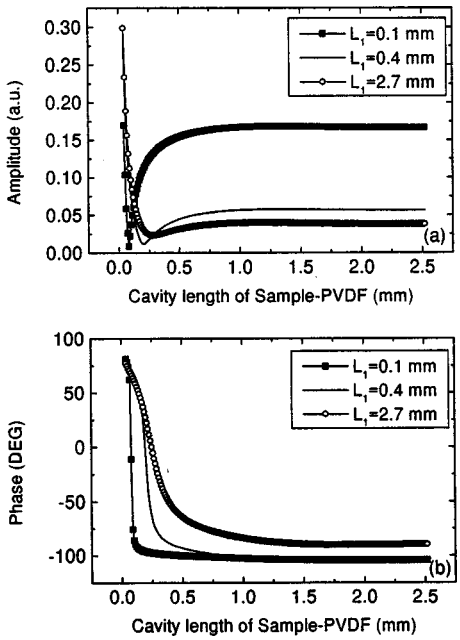

FIG. 6. Theoretical effect of reference-cavity length on the signal output of a PPE thermal-wave interferometer. The modulation frequency is $f=26.5$ Hz. The assumed values of the material parameters are the same as those used in Fig. 3 with $\Delta A=0.0113$.

B. Effect of the operating thermal-wave frequency

To optimize measurements, the characteristics of the PPE output signals under various modulation frequencies are calculated and shown in Fig. 7 using the parameters of Fig. 3. The cavity length L_1 is fixed at 0.2 mm. It can be seen from Fig. 7 that the signal dynamic range in both amplitude and phase channels at all frequencies considered in the simulation is comparable, however, sharper interferometric amplitude minima appear at lower frequencies. As a result, a low operating frequency should be employed, in order to produce a sharper interferometric ''dip'' and a higher-precision measurement. There is a limit in precision, however, since the lower modulation frequency will introduce a larger $1/f$ electronic noise leading to a degraded SNR. Therefore, in practice, the modulation frequency is usually chosen between 10 and 30 Hz. This frequency characteristic is also experimentally demonstrated in Figs. 8(a) and 8(b) at two

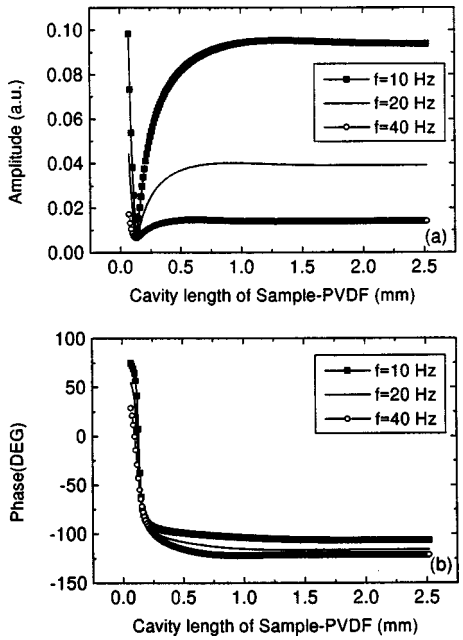

FIG. 7. Theoretical effect of modulation frequency on the PPE signal output of a thermal-wave interferometer. The reference is fixed at $L_1=0.2$ mm. The assumed values of the material parameters are the same as those used in Fig. 3 with $\Delta A=0.0113$.

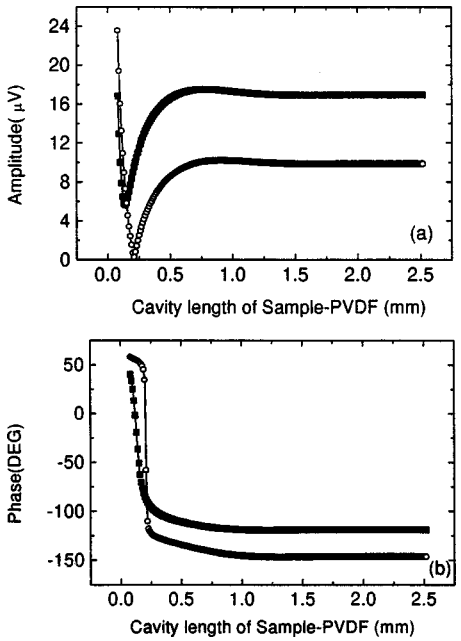

FIG. 9. Solid squares: theoretical curve fitted to the PPE experimental data of Fig. 3, $\Delta A=0.0113$; and open circles: using the same instrumental constant, and assuming $\Delta A=5\times10^{-4}$. Other parameters of the material are the same as those in Fig. 3.

different frequencies ($f=10$ and 26.5 Hz) using the same samples and experimental conditions as that in Fig. 5.

C. Measurement resolution

The maximum achievable differential-surface-absorptance, or bulk-absorption-coefficient resolution between the sample and the reference depends on the noise level of the output signal at the position of the interferometric minimum (dip). Theoretically, the output signal at the position of the minimum should be zero when the sample and the reference are identical (i.e., $\Delta A=0$, $\Delta\beta=0$, and $l=m$). If one of these optical parameters (e.g., surface absorptance) changes, $\Delta A\neq0$, the output signal at the dip is no longer equal to zero. Based on this nonzero dip output, we can obtain the small difference ΔA by means of a theoretical fit to the signal. The smallest measurable nonzero dip output will determine the maximum resolution of the measurement. Figure 9 shows the theoretical curve (solid squares) fitted to the experimental data in Fig. 3, from which the difference of the surface absorptance between the sample and the reference ($\Delta A=0.0113$) and an instrumental constant $S(26.5\,\text{Hz})=0.65126$ a.u., were obtained (see also Sec. III C). By using this instrumental constant and assuming a very small difference in the surface absorptance, $\Delta A=5\times10^{-4}$, the other theoretical curve (Fig. 9, open circles) was calculated. From this theoretical simulation, it was found that the output at the interferometric dip is approx. 0.5 μV. This level of PPE signal output is actually at the system noise limit in our present setup. Therefore, it is believed that the maximum resolution for measuring differential surface absorptance can reach the level of $\sim10^{-4}$.

A similar procedure can be followed to estimate the maximum resolution of the technique for measuring bulk absorption coefficient differences, $\Delta\beta$. In this case, the instrumental constant, $S(10\,\text{Hz})=0.31091$ a.u. was obtained from the best-fit results of Fig. 4. With the help of this instrumental constant, the theoretical curve in Fig. 10 was calculated using $\Delta\beta=2\times10^{-4}\,\text{cm}^{-1}$, so that the signal output would again be 0.5 μV, which is the system noise limit of our present setup. For maximum resolution, the reference was assumed to be fixed at $L_1=0.2$ mm (PPE mode). Therefore, $\sim10^{-4}\,\text{cm}^{-1}$ of differential bulk absorption can be considered as the maximum resolution for the pair of samples of

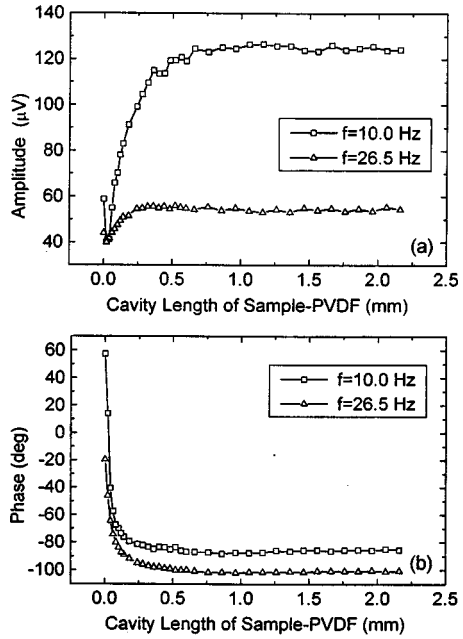

FIG. 8. Experimental demonstration of the effect of two different frequencies on the PPE interferometric signal using the same samples and experimental conditions as that in Fig. 5.

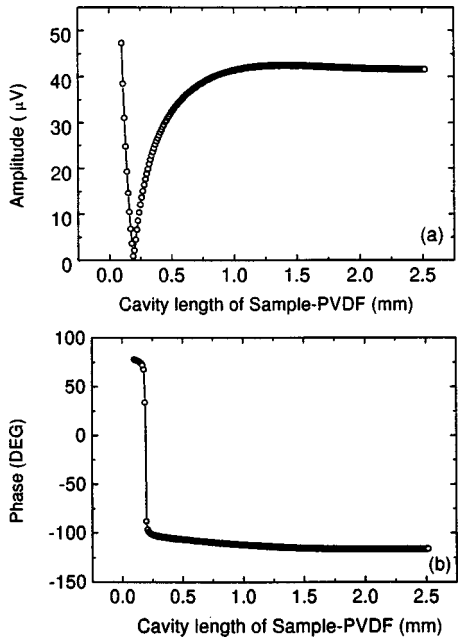

FIG. 10. Theoretical PPE signal output using the same instrumental constant as that in Fig. 4 and assuming $\Delta\beta = 2\times10^{-4}\ \mathrm{cm}^{-1}$. Other parameters of the material are the same as those in Fig. 3.

thickness ~2 cm. Nevertheless, the maximum possible resolution can easily reach 10^{-5}–$10^{-6}\ \mathrm{cm}^{-1}$ by using pairs of longer samples, say ⩾5 cm, or higher laser fluence.

Using the same estimation procedure for technique resolution regarding the absolute bulk absorption coefficient, if two transparent samples with thicknesses differing by one order of magnitude are used, the resolution can be estimated to be 10^{-5}–$10^{-6}\ \mathrm{cm}^{-1}$.

Based on the extension of our earlier purely thermal-wave photopyroelectric interferometric theory, the *differential* surface absorptance and *differential* bulk absorption coefficient, as well as the *absolute* bulk absorption coefficient of Ti:sapphire crystals have been separately and precisely measured using appropriate sample combinations. Owing to the destructive PPE interferometric effect, and unlike the conventional single-ended PPE technique, this interferometric method does not require precise knowledge of the remaining sample optical parameters to produce a high-precision measurement of one of optical parameters. The resolution limits for small differences in surface absorptance and bulk absorption coefficient were estimated to be $\sim10^{-4}$ and 10^{-5}–$10^{-6}\ \mathrm{cm}^{-1}$, respectively, with the current instrumental setup (the laser power is only ~5 mW). The resolution for low absolute bulk absorption coefficient was estimated to be 10^{-5}–$10^{-6}\ \mathrm{cm}^{-1}$. This is similar or even superior to other established, yet experimentally more involved photothermal techniques,[5,8] such as the photothermal deflection technique (PTD), in which a high-power pumping laser (~5 W) and a probing laser of a good Gaussian beam spot have to be employed and delicately adjusted with respect to the relative position of the position-sensing photodetector in order to obtain comparable resolution. In addition, a calibration process has to be conducted in PTD.[5,8] This new thermal-wave interferometric technique is expected to be useful in quality control of both bulk crystal growth and surface treatment of optical and laser crystals, thus impacting the performance of solid-state lasers.

ACKNOWLEDGMENT

The support of the Natural Sciences and Engineering Research Council of Canada (NSERC) through a Research Grant is gratefully acknowledged.

APPENDIX: DEFINITIONS OF EXPRESSIONS

$$N_1 \equiv 1 + \frac{R_s R_p (1-R_s)(1+R_s e^{-A_s}) e^{-2(\beta_s l + A_s)}}{1 - R_s^2 e^{-2(\beta_s l + A_s)}}, \tag{A1}$$

$$N_2 \equiv e^{-A_s}\left[R_s + \frac{R_p (1-R_s)(1+R_s e^{-A_s})}{1 - R_s^2 e^{-2(\beta_s l + A_s)}} \right], \tag{A2}$$

$$N_{1r} \equiv 1 + \frac{R_r R_p (1-R_r)(1+R_r e^{-A_r}) e^{-2(\beta_r m + A_r)}}{1 - R_r^2 e^{-2(\beta_r m + A_r)}}, \tag{A3}$$

$$N_{2r} \equiv e^{-A_r}\left[R_r + \frac{R_p (1-R_r)(1+R_r e^{-A_r})}{1 - R_r^2 e^{-2(\beta_r m + A_r)}} \right]. \tag{A4}$$

Also

$$I_t(0) = I_1 \frac{(1-R_s)e^{-A_s}}{1 - R_s^2 e^{-2(\beta_s l + A_s)}} (N_1 + N_2 e^{-2\beta_s l}), \tag{A5}$$

$$I_t(l) = I_1 \frac{(1-R_s)e^{-(\beta_s l + A_s)}}{1 - R_s^2 e^{-2(\beta_s l + A_s)}} (N_1 + N_2), \tag{A6}$$

$$I_{tr}(0) = I_2 e^{j\Delta\varphi} \frac{(1-R_r)e^{-A_r}}{1 - R_r^2 e^{-2(\beta_r m + A_r)}} (N_{1r} + N_{2r} e^{-2\beta_r m}), \tag{A7}$$

$$I_{tr}(m) = I_2 e^{j\Delta\varphi} \frac{(1-R_r)e^{-(\beta_r m + A_r)}}{1 - R_r^2 e^{-2(\beta_r m + A_r)}} (N_{1r} + N_{2r}), \tag{A8}$$

$$I_1(l) = I_1 \frac{(1-R_s)^2 e^{-(\beta_s l + 2A_s)}}{1 - R_s^2 e^{-2(\beta_s l + A_s)}}, \tag{A9}$$

$$I_2(m) = I_2 e^{j\varphi} \frac{(1-R_r)^2 e^{-(\beta_r m + 2A_r)}}{1 - R_r^2 e^{-2(\beta_r m + A_r)}}. \tag{A10}$$

The expressions for the constants H_1, H_2, G_3, and G_4 in Eq. (7) are

$$H_1 = (e^{\sigma_p d} - 1)(1 + \gamma_{gp} V_{34} e^{-2\sigma_g L_1}) + (1 - e^{-\sigma_p d})(\gamma_{gp} + V_{34} e^{-2\sigma_g L_1}), \tag{A11}$$

$$H_2 = (e^{\sigma_p d} - 1)(1 + \gamma_{gp} W_{21} e^{-2\sigma_g L}) + (1 - e^{-\sigma_p d})(\gamma_{gp} + W_{21} e^{-2\sigma_g L}), \tag{A12}$$

$$G_3 = \frac{2Q_1 e^{-\sigma_s l} - Q_2(1+b_{gs}) + Q_3(1-b_{gs}) e^{-2\sigma_s l}}{(1+b_{gs})^2 (1 - \gamma_{gs}^2 e^{-2\sigma_s l})}, \tag{A13}$$

with

$$Q_1 = E_s[b_{gs}(N_1 + N_2 e^{-2\beta_s l}) + r_s(N_1 - N_2 e^{-2\beta_s l})] + \eta_s^{(0)} A_s I_t(0)/(k_s \sigma_s), \tag{A14}$$

$$Q_2 = E_s e^{-\beta_s l}[N_1 + N_2 + r_s(N_1 - N_2)] - \eta_s^{(0)} A_s I_t(l)/(k_s \sigma_s), \tag{A15}$$

$$Q_3 = E_s e^{-\beta_s l}[N_1 + N_2 - r_s(N_1 - N_2)] + \eta_s^{(0)} A_s I_t(l)/(k_s \sigma_s), \tag{A16}$$

$$E_s = \frac{I_1 \eta_s^b \beta_s}{2k_s(\beta_s^2 - \sigma_s^2)} \cdot \frac{(1-R_s)e^{-A_s}}{1 - R_s^2 e^{-2(\beta_s l + A_s)}}, \tag{A17}$$

$$r_s = \beta_s / \sigma_s, \tag{A18}$$

and

$$G_4 = \frac{2P_1 e^{-\sigma_r m} + P_2(1+b_{gr}) - P_3(1-b_{gr})e^{-2\sigma_r m}}{(1+b_{gr})^2(1-\gamma_{gr}^2 e^{-2\sigma_r m})}, \tag{A19}$$

with

$$P_1 = E_r[b_{gr}(N_{1r} + N_{2r}e^{-2\beta_r m}) + r_r(N_{1r} - N_{2r}e^{-2\beta_r m})] + \eta_r^{(0)} A_r I_{tr}(0)/(k_r \sigma_r), \tag{A20}$$

$$P_2 = -E_r e^{-\beta_r m}[N_{1r} + N_{2r} + r_r(N_{1r} - N_{2r})] + \eta_r^{(0)} A_r I_{tr}(m)/(k_r \sigma_r), \tag{A21}$$

$$P_3 = -E_r e^{-\beta_r m}[N_{1r} + N_{2r} - r_r(N_{1r} - N_{2r})] - \eta_r^{(0)} A_r I_{tr}(m)/(k_r \sigma_r), \tag{A22}$$

$$E_r = \frac{I_2 e^{j\Delta\varphi} \eta_r^b \beta_r}{2k_r(\beta_r^2 - \sigma_r^2)} \cdot \frac{(1-R_r)e^{-A_r}}{1 - R_r^2 e^{-2(\beta_r m + A_r)}}, \tag{A23}$$

$$r_r = \beta_r / \sigma_r. \tag{A24}$$

[1] A. Mandelis and M. M. Zver, J. Appl. Phys. **57**, 4421 (1985).
[2] A. Mandelis, J. Vanniasinkam, S. Buddhudu, and M. Kokta, Phys. Rev. B **48**, 6808 (1993).
[3] J. Vanniasinkam, A. Mandelis, S. Buddhudu, and M. Kokta, J. Appl. Phys. **75**, 8090 (1994).
[4] J. Vanniasinkam, A. Mandelis, M. Munidasa, and M. Kokta, J. Opt. Soc. Am. B **15**, 1647 (1998).
[5] A. P. Kubyshkin, M. P. Matrosov, and A. A. Karabutov, Opt. Eng. (Bellingham) **33**, 3214 (1994).
[6] D. Dadarlat, M. Chirtoc, R. M. Candea, and I. Bratu, Infrared Phys. **24**, 469 (1984).
[7] A. C. Boccara, D. Fournier, W. Jackson, and N. H. Amer, Opt. Lett. **5**, 377 (1980).
[8] Y.-X. Nie and L. Bertrand, J. Appl. Phys. **65**, 438 (1989).
[9] A. Rosencwaig and T. W. Hidley, Appl. Opt. **20**, 606 (1981).
[10] J. Vanniasinkam, M. Munidasa, A. Othonos, M. Kokta, and A. Mandelis, IEEE J. Quantum Electron. **33**, 2301 (1997).
[11] J. Shen, K. Fjelsted, J. Vanniasinkam, and A. Mandelis, Opt. Mater. **4**, 823 (1995).
[12] S. Buddhudu, A. Mandelis, B. Joseph, and K. Fjelsted, Opt. Mater. **3**, 115 (1994).
[13] E. Welsch, in *Handbook of Optical Properties, Volume I, Thin Film for Optical Coatings*, edited by R. E. Hummel and K. H. Guenther (CRC, Boca Raton, FL, 1995), p. 243.
[14] A. Mandelis, R. E. Wagner, K. Ghandi, R. Baltman, and P. Dao, Phys. Rev. B **39**, 5254 (1989-I).
[15] C. Christofides, K. Ghandi, and A. Mandelis, Meas. Sci. Technol. **1**, 1363 (1990).
[16] C. Christofides, A. Mandelis, K. Ghandi, and R. E. Wagner, Rev. Sci. Instrum. **61**, 2360 (1990).
[17] C.-H. Wang and A. Mandelis, *Proceedings of the X International Conference on Photoacoustic Photothermal Phenomena*, edited by F. Scudieri (AIP, New York, 1998), p. 138.
[18] C.-H. Wang and A. Mandelis, J. Appl. Phys. **85**, 8366 (1999).
[19] C.-H. Wang and A. Mandelis, Rev. Sci. Instrum. (in press).
[20] M. R. Kokta, in *Tunable Solid-State Lasers II*, edited by A. B. Budgor, L. Esterowitz, and L. G. De Shazer (Springer, New York, 1986), p. 89.
[21] J. F. Pinto, L. Esterowitz, G. H. Rosenblatt, M. Kokta, and D. Peressini, IEEE J. Quantum Electron. **30**, 2612 (1994).
[22] P. H. Klein, *Physical Properties of Optical Materials* (SPIE, Bellingham, WA, 1979), Vol. 204, p. 77.